The preparation and characterisation of H_1-e palladium films with a regular hexagonal nanostructure formed by electrochemical deposition from lyotropic liquid crystalline phases

P. N. Bartlett, B. Gollas, S. Guerin and J. Marwan

Department of Chemistry, University of Southampton, Southampton, UK SO17 1BJ

The hexagonal (H_1) lyotropic liquid crystalline phases of $C_{16}EO_8$ (octaethyleneglycol monohexadecyl ether) and Brij® 56 non-ionic surfactants have been used to template the electrochemical deposition of nanostructured palladium films. The resulting H_1-e palladium films were characterised by SEM, TEM and X-ray. The films contain regular hexagonal arrays of cylindrical pores separated by palladium walls with a centre to centre distance of 5.8 nm. Electrochemical studies show that these films have very high surface areas of the order of 91 $m^2\ g^{-1}$. Studies of the hydrogen evolution reaction on these H_1-e palladium films in acid show that the formation of adsorbed hydrogen can be readily distinguished because of the high surface area to volume ratio of the films (of the order of $10^7\ cm^2\ cm^{-3}$). Hydrogen insertion into the palladium films is fast and the formation of both the α and β-hydride phases is observed in the voltammetry at potentials which are similar to those reported for bulk palladium. The electrodes are stable towards repeated cycling to form the β-hydride phase showing that the hydrogen insertion and concomitant lattice expansion does not destroy the H_1 nanostructure.

Introduction

The fabrication of nanostructured materials using surfactant molecules as templates has proved to be a very productive area of research since the early work on the formation of mesoporous silicas. Typically in this work relatively low concentrations of surfactants are employed which are believed to interact with the growing silica structures leading to the formation of materials with regular arrays of pores on the nanometre scale.[1–4] The success in fabrication of nanostructured silicas and modified silicas has been a stimulus to work in the use of template approaches to the fabrication of nanostructured materials and in the last few years there has been much effort to extend this approach to the fabrication of non-silicaceous materials.[5] In Southampton, starting with the work of Attard *et al.* on nanostructured silica,[6,7] we have developed a method which employs much higher concentrations of the surfactant (typically of the order of 50 wt.%) so that the fabrication of the nanostructured material takes place from a lyotropic liquid crystalline phase in a process which can be described as true liquid crystal templating. This approach has several significant advantages. First it is not restricted to the formation of silica; the method can be used to form a wide range of different nanostructured materials. Second the nanostructure of the final material is determined by the structure of the lyotropic liquid crystalline phase, consequently the dimensions and topology of the structure can be varied in a predictable fashion by the choice of surfactant and by the addition of co-solvents, based upon knowledge of the phase behaviour of the system. Third a wide range of different lyotropic phases exist with varying topologies which can be exploited in this fashion. Fourth the method can be use to produce nanostructured materials both by chemical and by electrochemical means. The latter approach has the additional advantages that it can be used to form nanostructured films at electrode surfaces, the thickness of the films being directly controlled through the amount of charge passed to carry out the deposition.

We have been particularly interested in the electrochemical deposition of nanostructured materials from lyotropic liquid crystalline phases of non-ionic surfactants. Using this approach we have deposited films of platinum,[8–13] cobalt,[14] tin,[15] metal alloys,[16] semiconductors[17] and polymers.[18] Using the platinum system we have shown that by electrochemical deposition from the hexagonal phase (H_1) we can produce platinum films with regular arrays of nanometre sized continuous pores arranged in a regular hexagonal array with wall thicknesses again of the order of nanometres. We refer to these as H_1-e films to denote the fact that they have a regular nanostructure and are formed by electrochemical deposition from the H_1 lyotropic liquid crystalline phase. The size of these pores and the thickness of the platinum walls can be varied by varying the alkyl chain length of the surfactant and by adding heptane as a co-solvent to swell the micellar surfactant rods in the lyotropic liquid crystalline phase. We have further shown that we can prepare platinum films with different topologies from other lyotropic phases and that the very high surface area of these films (of the order of $5 \times 10^6\ cm^2\ cm^{-3}$ corresponding, for platinum to a specific surface area of the order of 22 $m^2\ g^{-1}$) can be used as electrode materials for the measurement of oxygen,[19] hydrogen peroxide[20] or in electroanalysis.[10] Nanostructuring of metal films can also be used to control their physical properties, as illustrated by our recent work on H_1-e cobalt where we have shown that the coercivity of films can be controlled by varying the size of the nanostructure.[14]

In this paper we report the deposition of nanostructured palladium by electrochemical reduction of palladium ions dissolved in the aqueous domains of a hexagonal lyotropic liquid crystalline phase (H_1-e Pd). In the first part of the paper we describe the phase behaviour for the plating system and the characterisation, by X-ray diffraction, scanning electron microscopy, and transmission electron microscopy, of the nanostructured H_1-e palladium films. In the second part of the paper we describe the electrochemical behaviour of this

nanostructured material. Outside of the deposition of nanoparticles of Pd on conducting supports, there has not been a great deal of work reported on the preparation of nanostructured Pd films. In a recent paper Kang et al. described the chemical synthesis of some nanostructured palladium samples by infiltration of the pores of nanostructured samples of cubic MCM-48 and hexagonal SBA-15 nanostructured silicas with a palladium salt and subsequent reduction to the metal.[21] Although they characterised the nanostructured metal powders produced in this way they did not investigate the electrochemical properties. Guerin and Attard have reported the deposition of H_1-e platinum palladium alloys together with some studies of their electrochemistry.[22]

The electrochemistry of palladium differs significantly from that of platinum because palladium is able to absorb large quantities of hydrogen forming palladium hydride phases.[23] We were therefore particularly interested in the effects of the nanostructure of the palladium on this process. Previous work in the literature has shown that when thin films of palladium (of the order of a few nanometres in thickness) are used as electrodes the adsorption and absorption processes can be distinguished.[24–28] In addition there is evidence which suggests that for nanometre sized palladium particles the uptake of hydrogen into the metal is limited and is less than that for the bulk metal.[29]

Experimental

Hydrochloric acid (AnalaR BDH), sulfuric acid (AnalaR BDH), ammonium tetrachloropalladate (premion-99.998% Alfa Aesar), Brij® 56 (Aldrich), crystal violet (Aldrich), octaethyleneglycol monohexadecyl ether ($C_{16}EO_8$, Fluka) and heptane (99%, Lancaster) were all used as received. All aqueous solutions were freshly prepared using reagent grade water (18 MΩ cm resistance) from a Whatman "Stillplus" system coupled to a Whatman RO 50. All glassware used was soaked overnight in a 3% Decon/deionised water solution and washed thoroughly at least 3 times with deionised water prior to use.

All electrochemical experiments were carried out using an EG&G Model 263A potentiostat/galvanostat with a large area platinum gauze counter electrode and either a home-made saturated mercury sulfate reference electrode (SMSE) or home-made saturated calomel electrode (SCE). The counter electrode was a large area platinum gauze. The SMSE was used to avoid contamination of the sulfuric acid electrolyte solution used in the studies of the nanostructured palladium electrodes and all potentials are reported with respect to this reference electrode (the SMSE was found to be +0.448 V vs. SCE in 1 mol dm^{-3} H_2SO_4). The reference electrode was used in conjunction with a luggin capillary and stored in a saturated potassium sulfate solution when not in use.

The phase behaviour of the pseudobinary mixtures was investigated by polarised light microscopy using an Olympus BH-2 polarised light microscope equipped with a Linkam TMS90 heating stage and temperature control unit. Phases were assigned on the basis of their characteristic optical textures.[30] The phase transition boundaries were located to an accuracy of $\pm 2\,°C$ by using heating/cooling rates of $0.2\,°C$ min^{-1}.

The H_1-e Pd films were freshly prepared before each electrochemical experiment. For the electrochemical studies the H_1-e Pd films were deposited on to gold disc electrodes (area 0.0079 cm^2) formed by sealing 1 ± 0.1 mm diameter gold in glass. Immediately before use the gold disc electrodes were freshly polished using silicon carbide paper (Cc 1200, English Abrasives) and then alumina/water slurries (Beuhler) starting with a particle size of 25 μm and ending with a particles size of 0.3 μm. H_1-e Pd films were deposited onto the electrodes from solutions containing 12 wt.% $(NH_4)_2PdCl_4$, 47 wt.% surfactant (either Brij® 56 or $C_{16}EO_8$), 39 wt.% water and 2 wt.% heptane at 25 °C. The composition of the deposition solutions was chosen to correspond to that for the hexagonal (H_1) lyotropic phase as determined by studies of phase diagrams for the system. These deposition mixtures are highly viscous and must be prepared with care to ensure a uniform composition. After mixing all of the components the mixture was heated and stirred in order to ensure homogeneity and then cooled. The mixture was then checked using polarising light microscopy to ensure that it was in the hexagonal phase before use.

Palladium was deposited from the liquid crystalline plating mixture at 0.1 V vs. SCE. The total amounts of palladium deposited, assuming 100% faradaic efficiency for the process, were controlled by controlling the total amount of charge passed and was usually between 0.44 and 2.2 C cm^{-2} corresponding, respectively, to the deposition of between 1.9 μg and 9.7 μg of palladium onto the electrodes. The deposition took typically 150 s for the thinnest films. After deposition the Pd film was rinsed in purified water in order to remove the adhering surfactant mixture.

Electrochemical measurements on the H_1-e Pd films were carried out at room temperature (18–23 °C) in 1 M H_2SO_4. Before each experiment the solution was sparged for 10 to 15 min with a stream of highly purified argon gas to displace dissolved oxygen. The electrochemically active surface areas of the nanostructured palladium films were estimated by integrating the charge passed in the surface oxide stripping reaction recorded in 1 M sulfuric acid following the procedure suggested by Rand and Woods[31] and using their conversion factor of 424 μC cm^{-2}. In these experiments we cycled the potential between −0.65 and +0.7 V vs. SMSE at 20 mV s^{-1}.

Electrochemical quartz crystal microbalance (EQCM) measurements were carried out using polished, Au-coated, AT-cut 10 MHz quartz crystals with a diameter of 14 mm and a thickness of 0.168 mm sealed between two O-rings and forming the bottom of the cell made by Teflon. The apparatus used in these measurements has been described in detail elsewhere.[13] Briefly, the system applies a small frequency sweep about the resonant frequency of the crystal and measures the modulus of the crystal response. After the experiments the data was fitted to analytical expression for the complex voltage divider measurement of the transfer function modulus of the Butterworth van Dyke equivalent circuit for the quartz crystal electroacoustic impedance. This generated the values for the real and the imaginary components, R and X_L, of the electroacoustic impedance of the quartz crystal.

SEM images were obtained using a JOEL 300 scanning electron microscope. Samples for SEM analysis were prepared by electroplating Pd from the template mixture on to evaporated gold electrodes (area 1 cm^2) prepared by evaporation of a 10 nm thick layer of chromium (to ensure good adhesion) followed by 200 nm of gold on 1 mm thick glass microscope slides. These evaporated gold electrodes were cleaned in an ultrasonic bath of propan-2-ol for 10 min immediately before use. For transmission electron microscopy studies a JOEL 2000 TEM was used. The nanostructured Pd samples were strongly adherent on the gold electrode surface and samples for TEM analysis were prepared by scrapping small samples of palladium off of the evaporated gold electrode surface and on to the TEM grid using a scalpel.

Results

Phase behaviour

As demonstrated in our previous work, the nanostructures of the metal films deposited from the lyotropic phases of the non-ionic surfactant mixtures are directly determined by the
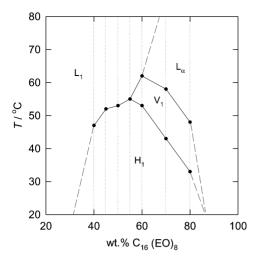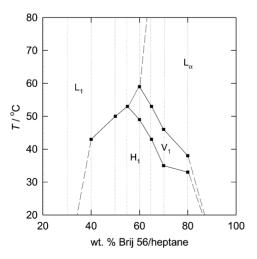
Fig. 1 Pseudobinary phase diagram of $C_{16}(EO)_8$ and water in which the concentration of $(NH_4)_2PdCl_4$ was kept fixed at 1.40 mol dm^{-3}. The dotted lines show the compositions that were investigated, while the lines denoting phase boundaries are drawn as guides to the eye. H_1 is the hexagonal phase, V_1 the cubic phase, L_α the lamellar phase and L_1 the micellar solution.

structure of the lyotropic phase used. We therefore begin by describing the phase behaviour of the mixtures of non-ionic surfactant and ammonium tetrachloropalladate solution. Two non-ionic surfactants were used in this work octaethyleneglycol monohexadecyl ether ($C_{16}EO_8$) and Brij® 56. $C_{16}EO_8$ is available as a highly purified, monodisperse, material whereas Brij® 56 is a polydisperse surfactant mixture with a distribution of headgroup sizes, the major components (>5%) being from $C_{16}EO_4$ to $C_{16}EO_{12}$ with $C_{16}EO_8$ as the most abundant. Fig. 1 shows the phase diagram obtained using mixtures of $C_{16}EO_8$ and ammonium tetrachloropalladate solution. The hexagonal, H_1, phase exists from between 30 to 40 wt.% $C_{16}EO_8$ up to 80 to 90 wt.% and is stable up to 55 °C for compositions around 55 wt.% $C_{16}EO_8$. The bicontinuous cubic, V_1, phase has a smaller region of existence between 55–60 wt.% and 80–90% $C_{16}EO_8$ at higher temperatures than the hexagonal phase. There is no evidence for the existence of the bicontinuous cubic phase at room temperature. At high concentrations of $C_{16}EO_8$ the lamellar, L_α, phase predominates. In the case of Brij® 56, Fig. 2, similar phase behaviour

is observed, with a similar, large region of the phase diagram occupied by the hexagonal, H_1, phase. However in this case the hexagonal phase is stable to slightly higher temperatures, up to 62 °C at between 40 and 55 wt.% surfactant. In contrast the bicontinuous cubic phase has a slightly reduced range of stability. Slight variations in composition occur between different batches of Brij® 56. Measurements using two different batches of material showed essentially the same phase behaviour when mixed with ammonium tetrachloropalladate solutions except that there was a variation of ±2 °C in the positions of the hexagonal/cubic and cubic/lamellar phase boundaries.

The phase behaviour found here for the $C_{16}EO_8$ ammonium tetrachloropalladate solution is almost identical to that for the $C_{16}EO_8$ water system reported by Mitchell *et al.*[30] and contrasts with the corresponding results found for $C_{16}EO_8$ with hexachloroplatinate solutions[9] where large changes in the locations of the stable regions of the different phases were observed. In the case of the hexachloroplatinic acid solutions these changes have been ascribed to interactions between the hexachloroplatinate anion and the ethylene oxide head groups of the surfactant leading to increased head group repulsion and stabilisation of those phases with a high positive mean curvature. For the tetrachloropalladate anion this does not appear to occur.

Both phase diagrams, Figs. 1 and 2, shows large composition and temperature ranges over which the hexagonal phase is stable and the compositions of the palladium deposition mixtures were chosen to correspond to the hexagonal phase. In each case the presence of the homogeneous hexagonal phase was confirmed by polarising light microscopy prior to palladium deposition. Fig. 3 illustrates the principle of this templated approach to the deposition of the nanostructured films. The metal salt is dissolved in the aqueous regions of the mixture around the hexagonally packed cylindrical
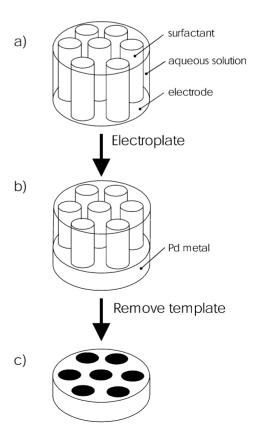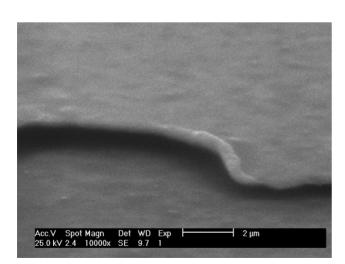

Fig. 2 Pseudobinary phase diagram of Brij® 56/heptane (ratio 22:1 by weight) and water in which the concentration of $(NH_4)_2PdCl_4$ was kept fixed at 1.40 mol dm^{-3}. The dotted lines show the compositions that were investigated, while the lines denoting phase boundaries are drawn as guides to the eye. H_1 is the hexagonal phase, V_1 the cubic phase, L_α the lamellar phase and L_1 the micellar solution.

Fig. 3 Schematic representation of the templating process used to deposit the H_1-e Pd films. The cylinders represent the micellar rods in the lyotropic liquid crystalline phase.

surfactant micelles (Fig. 3a). The electrochemical deposition of the metal then occurs in these regions producing a metal film around the surfactant micelles (Fig. 3b). After deposition the surfactant is simply removed by washing the films in water (see below) to leave the adherent, nanostructured metal film (Fig. 3c) as a direct cast of the lyotropic liquid crystalline phase.
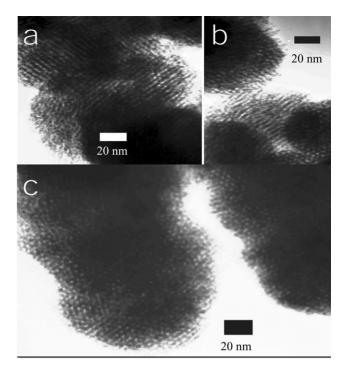
In this case the H_1-e Pd films were deposited at a constant potential of 0.1 V vs. SCE. At this potential the rate of deposition is controlled by the kinetics of the process and not by mass transport. The thickness of the deposited film was controlled by varying the total charge passed during deposition. Measurements using the electrochemical quartz crystal microbalance (EQCM) showed that the faradaic efficiency for deposition of palladium from the lyotropic liquid crystalline phase under these conditions was between 95 and 98%.

Characterisation of the H_1-e Pd films

Fig. 4 shows an SEM image of an H_1-e Pd film which is starting to lift away from the substrate. The film is smooth and dense with no evidence of the ordered nanostructure visible on the SEM scale. Fig. 5 shows a selection of TEM images from samples of H_1-e Pd scraped from the electrode surface. This image shows a highly porous structure consisting of cylindrical pores arranged on a hexagonal lattice. In Fig. 5a and b we can see regions in which there are side on views of the pores whereas Fig. 5c shows an end on view illustrating the hexagonal packing of the pores. From the TEM images we estimate that the material has a pore centre to pore centre distance of 5.8 nm with a pore diameter of about 3 nm and a wall thickness of about 3 nm. The structures seen here in the TEM are very similar to those already reported for H_1-e films of platinum or cobalt.[8,11,14] The structure of the H_1-e Pd films was also investigated by X-ray diffraction. Low angle X-ray reflection confirms the presence of a regular nanostructure with a broad peak at a value of 2θ of about 1.75°, corresponding to pore centre to pore centre distance of 5.8 nm in good agreement with the TEM data. Wide angle X-ray studies confirm that the palladium in the walls of the nanostructure is polycrystalline with the expected face centred cubic structure. From the widths of the X-ray peaks, using the Scherrer equation,[32] we estimate the grain size of the Pd to be around 20 nm.
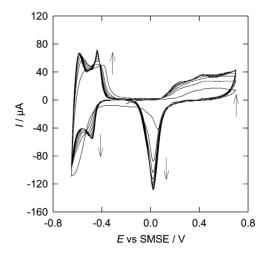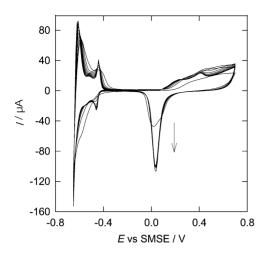
Fig. 5 Transmission electron micrograph of a sample scraped from an H_1-e Pd film deposited from the $C_{16}(EO)_8$ under the same conditions as Fig. 4.

Electrochemical measurements

Cyclic voltammetry in acid solutions was used to characterise the electrochemically active surface area of the H_1-e Pd films from the charge passed for stripping the surface oxide. When the films are deposited from the lyotropic liquid crystalline phase the pores in the palladium are initially filled by the surfactant. Superficial washing removes the surfactant from the outside of the film but it takes more prolonged washing in water to remove the surfactant from the pores. Fig. 6 shows a set of voltammograms for a freshly prepared H_1-e Pd film which was washed in water for 10 min then transferred to 1 M sulfuric acid solution. On the anodic sweep starting from 0.1 V we see the formation of the surface oxide. On the return, cathodic, sweep at around 0.05 V this surface oxide is removed

Fig. 4 Scanning electron micrograph of an H_1-e Pd film deposited on an evaporated gold electrode. The film was deposited from a mixture of 12 wt.% $(NH_4)_2PdCl_4$, 47 wt.% $C_{16}EO_8$, 2 wt.% heptane and 39 wt.% water. The total charge passed was 0.53 C cm^{-2} and the image was obtained at a tilt angle of 70°.

Fig. 6 Cyclic voltammograms of an H_1-e Pd film (200 nm thick, deposited from the Brij® 56 plating bath, total deposition charge 3.5 mC) deposited on a gold disc electrode (area 0.0079 cm^2) recorded at 20 mV s^{-1} in 1 M H_2SO_4. The film was soaked in water for 10 min immediately before the start of the voltammetry.

Fig. 7 Cyclic voltammograms of an H_1-e Pd film (200 nm thick, deposited from the Brij® 56 plating bath, total deposition charge 3.5 mC) deposited on a gold disc electrode (area 0.0079 cm²) recorded at 20 mV s⁻¹ in 1 M H_2SO_4. The film was soaked in water for 1 h before the start of the voltammetry.

giving rise to the well defined stripping peak in the voltammetry. These features are very similar to those seen for bulk polycrystalline palladium electrodes under the same conditions.[33] The peaks in the voltammetry at more negative potentials are associated with the formation of absorbed and adsorbed hydrogen and we shall return to these below. Looking at the peaks for formation and stripping of the surface oxide we see that these increase in size with each successive cycle. This occurs as the surfactant, originally in the pores within the H_1-e Pd film, diffuses out and is replaced by the 1 M sulfuric acid solution. As this happens the total surface area of palladium in contact with the acid solution increases and as a result the total electroactive surface area, as determined from the charge associated with the formation and removal of the surface oxide layer, increases. This interpretation is confirmed by the results in Fig. 7 which show a set of cyclic voltammograms recorded for an H_1-e Pd film which was first soaked in water for 1 h. In this case the charge associated with the removal of the surface oxide stabilises after only one cycle showing that the pores were no longer initially occupied by the surfactant. The changes in the voltammetry between the first and subsequent cycles in Fig. 7 are associated with the soaking in of the 1 M sulfuric acid into the water filled pores and to cleaning of the palladium surface. Experiments using thicker H_1-e Pd films show that, as expected, the time required to wash all of the surfactant from the pores increases as the thickness of the film increases and the pores become longer. Thus whilst soaking for 1 h is sufficient for a film that is approximately 200 nm thick it takes more than 4 h for a 1 μm thick film.

The voltammetry of polycrystalline palladium in 1 M sulfuric acid has been investigated by Rand and Woods.[31] Using their conversion factor of 424 μC cm⁻² for the oxide stripping peak we can estimate the electrochemically active surface area for our H_1-e Pd films assuming that the surface oxide formed on our nanostructured palladium electrodes is the same as that formed on bulk palladium. When we do this, and taking into account the measured faradaic efficiency for the deposition of the H_1-e Pd, we obtain specific surface areas for our films of around 91 m² g⁻¹. This corresponds to an area per unit volume of 1.1×10^7 cm² cm⁻³, a value which is consistent with the nanostructure found by TEM and X-ray and confirms that the entire sample is nanostructured with the pores throughout the film being accessible to the electrolyte solution.

EQCM measurements on the H_1-e Pd films during cycling in 1 M sulfuric acid show that dissolution of palladium, as determined by a decrease in mass of the electrode, starts with the formation of the surface oxide at around 0.1 V vs. SMSE on the anodic cycle and continues until around 0.05 V on the cathodic scan when the oxide is stripped from the electrode surface. This behaviour is identical to that reported for bulk polycrystalline electrodes[33] and is one reason why the oxide stripping charge, as opposed to the charge passed to form the oxide layer is used as a measure of the electrode surface area. In order to avoid any significant degradation of the nanostructure of the H_1-e Pd films caused by this dissolution and any subsequent replating of palladium on the cathodic cycle, freshly prepared electrodes soaked in water to remove the surfactant were used in the following studies, and we were careful to avoid repeatedly cycling the electrodes into the oxide formation region.

Hydrogen electrode reaction on nanostructure palladium

The evolution of hydrogen on palladium, as with other platinum group metals, is a multistep reaction which can be described by a Volmer–Heyrovsky–Tafel mechanism.[34–36] The first step in this process is the formation of adsorbed hydrogen atoms on the metal surface (the Volmer reaction)

$$H_3O^+ + e^- \rightarrow H^\bullet_{ads} + H_2O \qquad (1)$$

where $H^\bullet_{ads}$ is an adsorbed hydrogen atom at the metal surface. This is followed by either combination of two adsorbed hydrogen atoms to give molecular hydrogen (the Tafel reaction)
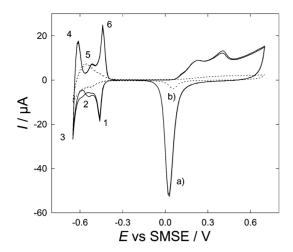
$$H^\bullet_{ads} + H^\bullet_{ads} \rightarrow H_2 \qquad (2)$$

or by a further electrochemical reaction (the Heyrovsky reaction)

$$H^\bullet_{ads} + H_3O^+ + e^- \rightarrow H_2 + H_2O \qquad (3)$$

where the relative importance of the Tafel and the Heyrovsky routes depends on the electrode potential. For palladium electrodes this picture is complicated by the absorption of hydrogen atoms into the bulk of the metal to form either the α or β hydride phases. At present there is no clear consensus about the mechanism by which the hydrogen enters the metal,[35,36] and in particular whether the adsorbed hydrogen atoms formed in the Volmer reaction are intermediates in the process. It has been suggested in the literature that a sub-surface layer of sorbed hydrogen may be involved.[28,37–39]
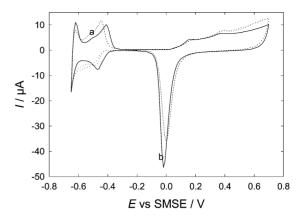
Fig. 8 shows a direct comparison of a H_1-e Pd film and a plain palladium film deposited from aqueous solution using the same charge, so that the total amount of palladium deposited onto the 1 mm diameter gold electrode was the same in each case. Several striking differences are immediately apparent. First the charge passed to deposit and to strip the surface oxide is much larger for the H_1-e Pd film than for the corresponding plain film, yet the oxidation and reduction processes occur at the same potentials for the two films. This difference arises because the H_1-e Pd film has a much greater surface area because of the dense array of cylindrical pores puncturing the film. Second, at cathodic potentials the two voltammograms differ significantly. The H_1-e Pd film exhibits a very sharp pair of peaks (denoted as peaks 1 and 6 in the figure) around -0.45 V vs. SMSE with a smaller, broader pair of peaks (2 and 5) at -0.52 V vs. SMSE and then a rapidly increasing reduction current at the cathodic limit of the sweep associated with a peak in the oxidation current at -0.625 V vs. SMSE (3 and 4) on the return scan. In contrast voltammetry of the plain palladium film is broad and unresolved in this region. Similar results were obtained for a polycrystalline palladium wire (not shown). Clearly this difference in voltammetry between the
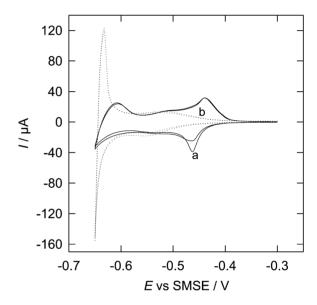
Fig. 8 Cyclic voltammograms recorded at 20 mV s^{-1} in 1 M H$_2$SO$_4$ for (a) an H$_1$-e Pd film deposited from the Brij$^{®}$ 56 plating mixture and (b) a plain Pd film deposited from an aqueous solution containing 50 mM (NH$_4$)$_2$PdCl$_4$, 1 M HCl and 1 M NH$_4$Cl. In both cases the films were deposited on 1 mm diameter gold electrodes with a deposition charge of 3.5 mC.

Fig. 9 Cyclic voltammograms of an H$_1$-e Pd film deposited from the Brij$^{®}$ 56 plating solution onto a gold disc electrode (1 mm diameter, deposition charge 3.5 mC). The voltammograms were recorded at 20 mV s^{-1} in (a) 0.1 M H$_2$SO$_4$ and (b) 0.1 M HClO$_4$.
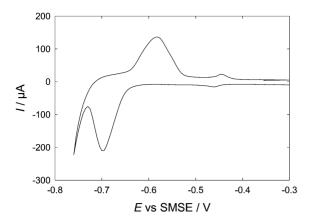

Fig. 10 Cyclic voltammograms for a 200 nm thick H$_1$-e Pd film deposited onto a 1 mm diameter gold electrode recorded at 20 mV s^{-1} in 1 M H$_2$SO$_4$ without (curve a) and with (curve b) 1 mM crystal violet present

H$_1$-e film and the plain film is due to the presence of the nanostructure.

The well resolved pair of peaks for the H$_1$-e Pd film (1 and 6) correspond to the formation and removal of adsorbed hydrogen atoms at the palladium surface, reaction (1) above. Similar, although not as well resolved, peaks have been observed by Baldaulf and Kolb in studies of thin (1 to 10 monolayer equivalent) palladium films deposited on gold single crystals[27] and for small palladium particles supported on carbon electrode surfaces.[40] In both cases the peaks for the adsorbed hydrogen can be resolved for thin films or small particles because the current for the formation of absorbed hydrogen does not dominate the voltammetry as it does for bulk palladium electrodes. Confirmation for this assignment was provided by Baldauf and Kolb who showed that the mid-peak potential for the adsorbed H couple varied with proton concentration but not anion concentration, that very similar voltammetry was observed for sulfuric and perchloric acids, and that addition of crystal violet to the solution totally suppressed the hydrogen adsorption. For our H$_1$-e Pd films it was not possible to go to proton concentrations much below 0.1 M without encountering significant distortion in the voltammetry. This arises because of the very significant concentration changes which can be expected to occur within the narrow pores in the structure during the voltammetry. For example if we take the charge passed in the peaks 1 and 6 in Fig. 8 and convert this to the corresponding change in proton concentration within the pores of the nanostructure we find that this corresponds to a change of the order of several molar in proton concentration. In addition at low electrolyte concentrations or at high sweep rates the voltammetry can be distorted by the iR drop occurring along the pores. This effect has been studied for H$_1$-e Pt films by Elliott and Owen.[12] Despite these problems, we have investigated the concentration dependence of the mid peak potential for peaks 1 and 6 over a limited proton concentration range and find that it agrees with the results of Baldaulf and Kolb. Fig. 9 shows typical voltammograms for an H$_1$-Pd film in 0.1 M sulfuric acid and 0.1 M perchloric acid. Comparing the results to those in Fig. 8 we notice that there is a slight shift in the mid peak potentials in going from 1 M to 0.1 M sulfuric acid. In addition we see that changing from sulfate to perchlorate has little effect on the voltammetry beyond a small shift which can be accounted for by the difference in pH of the two solutions. Finally we have investigated the effect of crystal violet on the voltammetry, Fig. 10. Again our results

are very similar to those reported by Baldaulf and Kolb. In the presence of 1 mM crystal violet the peaks 1 and 6 are totally suppressed confirming that they arise from the formation of adsorbed hydrogen at the electrode surface. Based on the total charge passed for the formation of the adsorbed hydrogen, and comparing this to the corresponding oxide stripping charge, we estimate the coverage to be 0.20 H per surface palladium atom.
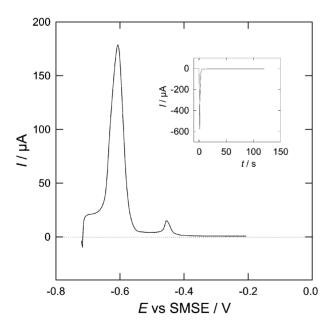
Absorption of hydrogen into H$_1$-e Pd films

The remaining two pairs of peaks (2–5, and 3–4) in Fig. 8 are associated with the formation of absorbed hydrogen and correspond to the formation of the Pd α-hydride and the start of the formation of the β-hydride phase. When the potential is scanned further cathodic, Fig. 11, we can clearly see that peaks 3 and 4 of Fig. 8 become the two large peaks associated with the formation and oxidation of the β-hydride phase. In order to investigate the formation of the hydride phases in

Fig. 11 Cyclic voltammogram of an H_1-e Pd film deposited from the Brij® 56 plating solution onto a gold disc electrode (1 mm diameter, deposition charge 3.5 mC) recorded at 10 mV s^{-1} 1 M H_2SO_4.
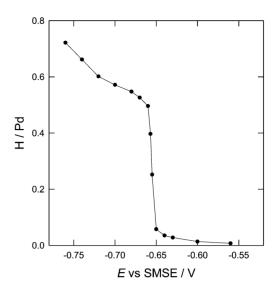

Fig. 13 Plot of the H/Pd ratio as a function of potential for an H_1-e Pd film. The hydrogen loading of the electrode was determined from anodic voltammetric sweeps of the type shown in Fig. 12 after stepping the electrode to different cathodic potentials. The total palladium loading was calculated from the charge passed to deposit the H_1-e Pd film (7 mC for 1 mm diameter electrode) and the measured faradaic efficiency for the deposition.

more detail we carried out a series of experiments in which the potential of the electrode was stepped from 0.56 V to increasingly cathodic potentials, held at the cathodic potential for 120 s and then swept back at 10 mV s^{-1}. In a separate set of experiments the length of time that the electrode was held at the cathodic potential was varied in order to ensure that sufficient time was allowed for the system to equilibrate at the cathodic potential before the anodic sweep. Fig. 12 shows a typical voltammogram for the reverse sweep while the inset shows the current transient for the initial potential step. It is clear from the transient that the reduction process occurs rapidly and is complete after 120 s. This reduction corresponds to the reduction of protons and the formation of the absorbed hydrogen atoms in the palladium. It is notable that this process occurs much more rapidly for the H_1-e Pd films than for thin Pd films studied in the literature.[24] On the reverse voltammetric sweep,

Fig. 12 Example of a voltammogram for the oxidation of hydrogen absorbed and adsorbed on an H_1-e Pd film in 1 M H_2SO_4 recorded at 10 mV s^{-1}. The electrode was stepped from -0.2 to -0.72 V vs. SMSE and held there for 120 s to load the electrode with hydrogen immediately before the anodic scan. The inset shows the corresponding current transient for loading the electrode with hydrogen at -0.72 V. The H_1-e Pd film was deposited from the Brij® 56 plating bath onto a 1 mm diameter gold disc electrode (charge passed 3.5 mC).

Fig. 12 (main part), there are two well resolved peaks. The peak at -0.6 V vs. SMSE corresponds to the oxidation of the β-hydride, while the peak at -0.453 V vs. SMSE corresponds to the oxidation of adsorbed hydrogen at the palladium surface and occurs at around the same potential as peak 6 in Fig. 8 We also note that the resolution of the peaks in the voltammogram in Fig. 12 is much better than that reported by Czerwinski et al. in similar experiments carried out for thin Pd films again indicating that the processes are more rapid at the H_1-e Pd films.

By carrying out a series of experiments of the sort shown in Fig. 12 in which the potential was stepped to different cathodic values and then integrating the total charge passed in the anodic sweep we can build up a plot of the charge as a function of potential. This charge can then be converted into the ratio of hydrogen to palladium at each potential by using the total charge passed to deposit the palladium film together with the measured faradaic efficiency for the deposition. The resulting plot is shown in Fig. 13. Below -0.55 V vs. SMSE the H/Pd ratio increases slowly as the potential becomes more cathodic. This corresponds to the formation of the α-hydride phase which is stable up to H/Pd less than about 0.05.[41] The sharp rise in the H/Pd ratio at -0.653 V vs. SMSE (equivalent to 0.046 V vs. SHE) corresponds to the formation of the β-hydride phase. This result is consistent with that of Czerwinski et al.[24] for thin films of Pd (300 to 500 monolayer equivalents) deposited onto gold electrodes who found that the transition from the α to β phase occurred at -0.230 V vs. SCE in 0.5 mol dm^{-3} H_2SO_4. However in comparison to their data we find that for the H_1-e Pd film the phase transition occurs over a significantly smaller potential range ($\sim$20 mV as compared to $\sim$50 mV). At more cathodic potentials the H/Pd ratio in Fig. 13 tends towards a plateau at around 0.59 before increasing again at potentials more cathodic than -0.71 V. The plateau value of 0.59 presumably corresponds to the composition of the β-hydride phase formed by the H_1-e Pd film. This value is close to the value of 0.6 for the bulk β-hydride reported in the literature.[41] The further increase in the apparent H/Pd ratio in Fig. 13 below -0.71 V is unexpected and has not been reported before in the literature. If we return to Fig. 12 it is

clear that the apparent increase in H/Pd ratio occurs because of the additional contribution to the stripping charge from the current cathodic of the large peak associated with the oxidation of the β-hydride phase. From the voltammetry (Fig. 11 and Fig. 12) this current appears to be capacitive in origin and this could explain why we see this for the H_1-e Pd where the surface area of the electrode is very large compared to the volume of the metal although it is not clear why the double layer capacitance of the β-hydride should be so much greater than that of the Pd metal.

Two other interesting points arise from this study. First it is clear from our cyclic voltammetry results and potential step experiments that the formation of the β-hydride phase and its subsequent oxidation back to Pd does not destroy the nanostructure despite the fact that insertion of H into the metal to make the β phase is accompanied by a 3% expansion in the Pd lattice parameter.[41] Presumably this expansion can be accommodated by the nanostructure without it breaking up. Second we find that the thermodynamics of the formation of the α- and β-hydride phases are not significantly altered by the presence of the nanostructure, an observation which is consistent with the results above from X-ray studies which showed that the Pd in the walls of the H_1-e film has the same lattice parameters as bulk Pd. Third, the kinetics of the process are greatly enhanced so that we see a sharper phase transition as a function of potential; and more clearly defined voltammetric peaks for the reactions. This enhancement in the kinetics may be explained for the H_1-e Pd film because its geometry means that no point within the metal is more than a few nanometres from the surface. Consequently for these films we expect diffusion of H through the lattice in either α or β phases to be so fast as not to be rate limiting (the diffusion coefficients for H in the α and β phases are around 2×10^{-7} and 2×10^{-6} cm^2 s^{-1} respectively[42] so the time taken for an H atom to diffuse right the way through the nanostructure would be of the order of 20 ns) .

Conclusions

In this paper we have shown that we can prepare nanostructured H_1-e Pd films by electrochemical deposition from the hexagonal lyotropic liquid crystalline phases of either $C_{16}EO_8$ or Brij® 56. These films contain regular arrays of cylindrical pores about 3 nm in diameter arranged in an hexagonal array with 5.8 nm between the pore centres. Electrochemical studies show that these H_1-e Pd films have high electroactive specific surface areas of the order of 91 m^2 g^{-1} (corresponding to 1×10^7 cm^2 cm^{-3}). This high surface area structure is stable on cycling to cathodic potentials in acid solution and can be converted to the β-hydride phase and back to Pd without loss of nanostructure. Because of the very high surface to volume ratio of the H_1-e Pd and the fast kinetics for the formation of the α- and β-hydride phases we can readily distinguish the formation of adsorbed and absorbed H in the voltammetry of these films.

The electrochemical deposition of high surface area Pd films with regular, controlled, nanostructures opens up a number of potential applications. For example, high surface area Pd films are of particular interest as catalysts methane oxidation in gas sensors[43,44] and this will form the subject of a subsequent publication.

Acknowledgement

References

1 J. Liu, Y. Shin, Z. Nie, J. H. Chang, L.-Q. Wang, G. E. Fryxell, W. D. Samuels and G. J. Exarhos, *J. Phys. Chem. A*, 2000, **104**, 8328.
2 N. K. Raman, M. T. Anderson and C. J. Brinker, *Chem. Mater.*, 1996, **8**, 1682.
3 M. E. Raimondi and J. M. Seddon, *Liq. Cryst.*, 1999, **26**, 305.
4 Q. Huo, D. I. Margolese, U. Ciesla, D. G. Demuth, P. Feng, T. E. Gier, P. Sieger, A. Firouzi, B. F. Chmelka, F. Schüth and G. D. Stucky, *Chem. Mater.*, 1994, **6**, 1176.
5 F. Schüth, *Chem. Mater.*, 2001, **13**, 3184.
6 G. S. Attard, C. G. Göltner, J. M. Corker, S. Henke and R. H. Templer, *Angew. Chem., Int. Ed. Engl.*, 1997, **36**, 1315.
7 G. S. Attard, J. C. Glyde and C. G. Göltner, *Nature*, 1995, **378**, 366.
8 G. S. Attard, P. N. Bartlett, N. R. B. Coleman, J. M. Elliott, J. R. Owen and J. H. Wang, *Science*, 1997, **278**, 838.
9 G. S. Attard, P. N. Bartlett, N. R. B. Coleman, J. M. Elliott and J. R. Owen, *Langmuir*, 1998, **14**, 7340.
10 J. M. Elliott, P. R. Birkin, P. N. Bartlett and G. S. Attard, *Langmuir*, 1999, **15**, 7411.
11 J. M. Elliott, G. S. Attard, P. N. Bartlett, N. R. B. Coleman, D. A. S. Merckel and J. R. Owen, *Chem. Mater.*, 1999, **11**, 3602.
12 J. M. Elliott and J. R. Owen, *Phys. Chem. Chem. Phys.*, 2000, **2**, 5653.
13 B. Gollas, J. M. Elliott and P. N. Bartlett, *Electrochim. Acta*, 2000, **45**, 3711.
14 P. N. Bartlett, P. R. Birkin, M. A. Ghanem, P. de Groot and M. Sawicki, *J. Electrochem. Soc.*, 2001, **148**, C119.
15 G. S. Attard, J. M. Elliott, P. N. Bartlett, A. Whitehead and J. R. Owen, *Macromol. Symp.*, 2000, **156**, 179.
16 G. S. Attard, S. A. A. Leclerc, S. Maniguet, A. E. Russell, I. Nandhakumar, B. R. Gollas and P. N. Bartlett, *Microporous Mesoporous Mater.*, 2001, **44**, 159.
17 I. Nandhakumar, J. M. Elliott and G. S. Attard, *Chem. Mater.*, 2001, **13**, 3840.
18 J. M. Elliott, L. M. Cabuché and P. N. Bartlett, *Anal. Chem.*, 2001, **73**, 2855.
19 P. R. Birkin, J. M. Elliott and Y. E. Watson, *J. Chem. Soc., Chem. Commun.*, 2000, 1693.
20 S. A. G. Evans, J. M. Elliott, L. M. Andrews, P. N. Bartlett, P. J. Doyle and G. Denuault, *Anal. Chem.*, 2002, **74**, 1322.
21 H. Kang, Y.-W. Jun, J.-I. Park, K.-B. Lee and J. Cheon, *Chem. Mater.*, 2000, **12**, 3530.
22 S. Guerin and G. S. Attard, *Electrochem. Commun.*, 2001, **3**, 544.
23 F. Lewis, *The palladium–hydrogen system*, Academic Press, London, 1967.
24 A. Czerwinski, R. Marassi and S. Zamponi, *J. Electroanal. Chem.*, 1991, **316**, 211.
25 A. Czerwinski, S. Zamponi and R. Marassi, *J. Electroanal. Chem.*, 1991, **304**, 233.
26 A. Czerwinski, M. Czaudema, G. Maruszczak, I. Kiersztyn, R. Marassi and S. Zamponi, *Electrochim. Acta*, 1997, **42**, 81.
27 M. Baldauf and D. M. Kolb, *Electrochim. Acta*, 1993, **38**, 2145.
28 A. Czerwinski, I. Kiersztyn, M. Grden and J. Czapla, *J. Electroanal. Chem.*, 1999, **471**, 190.
29 N. K. Nag, *J. Phys. Chem. B*, 2001, **105**, 5945.
30 D. J. Mitchell, G. J. T. Tiddy, J. Waring, T. Bostock and M. P. McDonald, *J. Chem. Soc., Faraday Trans. 1*, 1983, **79**, 975.
31 D. A. J. Rand and R. Woods, *J. Electroanal. Chem.*, 1972, **35**, 209.
32 C. Giacovasso, *Fundamentals of Crytallography*, Oxford University Press, Oxford, 1992.
33 L. D. Burke and J. K. Casey, *J. Electrochem. Soc.*, 1993, **140**, 1284.
34 W.-S. Zhang, X.-W. Zhang and H.-Q. Li, *J. Electroanal. Chem.*, 1997, **434**, 31.
35 G. Mengoli, M. Bernardini, M. Fabrizio, C. Manduchi and G. Zannoni, *J. Electroanal. Chem.*, 1996, **403**, 143.
36 C. Lim and S.-I. Pyun, *Electrochim. Acta*, 1994, **39**.
37 M. W. Breiter, *J. Electroanal. Chem.*, 1980, **109**, 253.
38 B. E. Conway and G. Jerkiewicz, *J. Electroanal. Chem.*, 1993, **357**, 47.
39 R. V. Bucur and F. Bota, *Electrochim. Acta*, 1982, **27**, 521.
40 N. Tateishi, K. Yahikozawa, K. Nishimura, M. Suzuki, Y. Iwanaga, M. Watanabe, E. Enami, Y. Matsuda and Y. Takasu, *Electrochim. Acta*, 1991, **36**, 1235.
41 H. A. Rafizadeh, *Phys. Rev. B*, 1981, **23**, 1628.
42 V. Breger and E. Gileadi, *Electrochem. Acta*, 1971, **16**, 177.
43 C. F. Cullis and D. E. Keene, *J. Catal.*, 1970, **19**, 378.
44 C. F. Cullis and B. M. Willatt, *J. Catal.*, 1983, **83**, 267.